Localizing a gate in CFTR

Xiaolong Gao[a,b] and Tzyh-Chang Hwang[a,b,c,1]

[a]Dalton Cardiovascular Research Center and Departments of [b]Biological Engineering and [c]Medical Pharmacology and Physiology, University of Missouri–Columbia, Columbia, MO 65211

Edited by Christopher Miller, Howard Hughes Medical Institute, Brandeis University, Waltham, MA, and approved January 21, 2015 (received for review October 29, 2014)

Experimental and computational studies have painted a picture of the chloride permeation pathway in cystic fibrosis transmembrane conductance regulator (CFTR) as a short narrow tunnel flanked by wider inner and outer vestibules. Although these studies also identified a number of transmembrane segments (TMs) as pore-lining, the exact location of CFTR's gate(s) remains unknown. Here, using a channel-permeant probe, $[Au(CN)_2]^-$, we provide evidence that CFTR bears a gate that coincides with the predicted narrow section of the pore defined as residues 338–341 in TM6. Specifically, cysteines introduced cytoplasmic to the narrow region (i.e., positions 344 in TM6 and 1148 in TM12) can be modified by intracellular $[Au(CN)_2]^-$ in both open and closed states, corroborating the conclusion that the internal vestibule does not harbor a gate. However, cysteines engineered to positions external to the presumed narrow region (e.g., 334, 335, and 337 in TM6) are all nonreactive toward cytoplasmic $[Au(CN)_2]^-$ in the absence of ATP, whereas they can be better accessed by extracellular $[Au(CN)_2]^-$ when the open probability is markedly reduced by introducing a second mutation, G1349D. As $[Au(CN)_2]^-$ and chloride ions share the same permeation pathway, these results imply a gate is situated between amino acid residues 337 and 344 along TM6, encompassing the very segment that may also serve as the selectivity filter for CFTR. The unique position of a gate in the middle of the ion translocation pathway diverges from those seen in ATP-binding cassette (ABC) transporters and thus distinguishes CFTR from other members of the ABC transporter family.

cystic fibrosis | gating | ABC transporters | anion channels

To maintain cellular homeostasis and to exchange information between two sides of the plasma membrane that acts as an effective barrier for most hydrophilic molecules, two large classes of transport proteins—ion channels and active transporters—evolve to catalyze transmembrane movements of biologically important molecules. For both types of catalysts, this transport function requires a translocation pathway that spans the lipid bilayer. In the case of an ion channel, the transmembrane domain(s) affords a continuous permeation pathway once the gate opens, through which millions of selected ions can pass rapidly down their electrochemical gradient (1, 2). However, such an open pore model is unlikely to be adopted by active transporters, as these proteins have to move their substrates against a concentration gradient (3). Therefore, the alternating-access mechanism has been proposed for active transporters wherein an intracellular and an extracellular gate open and close alternately (4), hence avoiding a dissipation of the established concentration gradient. Recent crystallographic studies (5–8), by revealing detailed molecular structures of several active transporters, indeed support this flip-flop mode of action. Despite such dramatic differences in their modus operandi, at least two families of membrane proteins—ATP-binding cassette (ABC) protein superfamily and chloride channels (CLC) transporter/channel family—espouse both ion channels and active transporters, suggesting evolutionary transformations between channels and transporters (9).

Although classified into the ABC transporters superfamily (10), most members of which harness the energy from ATP hydrolysis to actively transport their substrates across the membrane, cystic fibrosis transmembrane conductance regulator (CFTR), whose malfunction leads to the genetic disease cystic fibrosis, is a phosphorylation-activated but ATP-gated chloride channel (11). Like many other members of this superfamily, CFTR possesses two transmembrane domains (TMD1 and TMD2), each of which comprises six transmembrane segments (TMs). At the end of each TMD lies a nucleotide binding domain (NBD1 and NBD2, respectively), which plays a critical role in controlling channel gating via ATP-induced NBD dimerization and hydrolysis-triggered separation of the dimer (12, 13). In addition, a regulatory domain (R domain), linking two TMD/NBD complexes, harbors multiple consensus sites for protein kinase A (PKA)-dependent phosphorylation (14). Decades of biochemical and biophysical studies of CFTR have provided exquisite insights into not only how the molecular events in NBDs are coupled to opening and closing of the gate in TMDs (13) but also how different TMs craft CFTR's ion-conducting pore (15–24). Specifically, studies using the substituted cysteine accessibility method (SCAM) have demonstrated that TM1, 3, 6, 9, 11, and 12 contribute to pore lining, with TM1, 6, and 12 intimately involved in gating motions of the TMDs (15, 16, 20, 25). Although the molecular structure of CFTR's TMDs remains to be solved, both electrophysiological studies (15, 20, 21) and computational modeling (22, 26, 27) support the view that CFTR's pore is made up of a narrow tunnel flanked by an inner and an outer vestibule (Fig. 1*A*). Despite much advance being made in the past decade from detailed structure/function studies of CFTR's TMDs, the location of its gate(s), defined as the part in the pore where ion flow stops when the channel closes, remains elusive.

As phylogenetic studies have grouped CFTR into the ABCC subfamily (10), whose members are mostly exporters, it is long speculated that CFTR could evolve from a primordial exporter by degenerating one of the two gates (i.e., intracellular gate and

Significance

Cystic fibrosis transmembrane conductance regulator (CFTR), albeit a bona fide member of the ATP-binding cassette (ABC) transporter superfamily, is an ATP-gated chloride channel. However, phylogenetic analysis has led to a popular conjecture that CFTR evolves from a primordial ABC exporter by simply degenerating the cytoplasmic gate. This degraded transporter hypothesis predicts that CFTR's gate is located at the external end of the substrate translocation pathway as the one documented in the crystal structures of ABC exporters. Here we provide experimental data supporting the presence of a gate in CFTR at a segment that may also serve as the selectivity filter. This functional duality of a restrictive segment close to the middle of the pore axis distinguishes CFTR from its myriad brethren in the ABC protein family.

Author contributions: X.G. and T.-C.H. designed research; X.G. performed research; X.G. analyzed data; and X.G. and T.-C.H. wrote the paper.

The authors declare no conflict of interest.

This article is a PNAS Direct Submission.

[1]To whom correspondence should be addressed. Email: HwangT@health.missouri.edu.

This article contains supporting information online at www.pnas.org/lookup/suppl/doi:10.1073/pnas.1420676112/-/DCSupplemental.

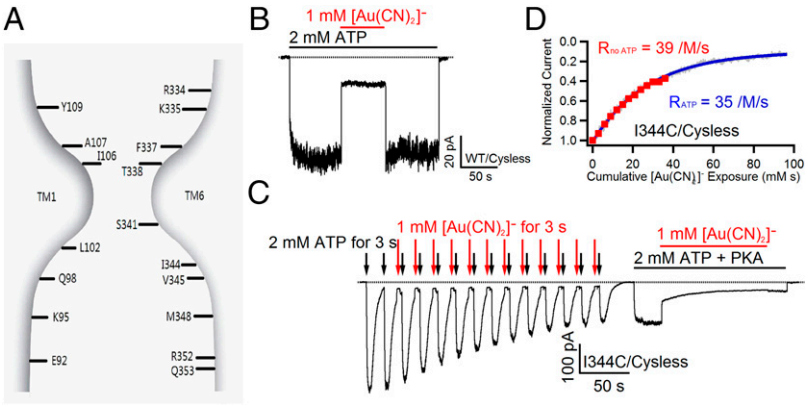

Fig. 1. Current understanding of CFTR's pore architecture and thiol-specificity of $[Au(CN)_2]^-$. (*A*) A cartoon depicting the essence of the pore of CFTR based on previous cysteine scanning studies (15, 17, 19–21). TM1 and TM6 are shown, as these two segments likely span the entire pore axis. Labeled positions mark the residues that actually contribute to pore-lining. (*B*) Reversible block of cysless WT-CFTR by 1 mM $[Au(CN)_2]^-$. (*C*) Reaction between I344C–CFTR and 1 mM $[Au(CN)_2]^-$ in the presence or absence of ATP (see *Results* for details). Note a two-step current decay when $[Au(CN)_2]^-$ was applied with ATP. (*D*) State-independent reactivity of I344C–CFTR to $[Au(CN)_2]^-$. Data extracted from *C*. Red squares represent normalized current amplitudes obtained from the first part of the trace shown in *C*, where $[Au(CN)_2]^-$ was applied without ATP, and the gray trace is the second phase (ligand exchange phase) of the current decay, when $[Au(CN)_2]^-$ was applied in the presence of ATP. Fitting these data with a single exponential function resulted in similar secondary reaction rates.

extracellular gate) (9, 28). Because NBD dimerization triggers gate opening in CFTR, it is further proposed that it is the intracellular gate that is degraded to convert an exporter to a channel (28). It follows that CFTR's gate is expected to reside at the external end of the pore, resembling the extracellular gate of its close cousins (6–8). Indeed, recent cysteine scanning studies did demonstrate a lack of an internal gate for CFTR (16, 18), but evidence supporting the presence of an external gate is scant. In an attempt to understand the molecular basis of CFTR gating, we decided to carry out more extensive SCAM studies using a channel-permeant probe, $[Au(CN)_2]^-$.

To localize the gate of CFTR, we targeted mainly TM6, as this TM has been shown to span the whole length of the anion permeation pathway (i.e., the inner and outer vestibules as well as the predicted narrow region; Fig. 1*A*) (15, 17, 21, 22). Cysteines introduced cytoplasmic to the predicted narrow region (e.g., residue 344) can be modified by intracellular $[Au(CN)_2]^-$ in both the open and the closed states, suggesting the lack of a "gate" cytoplasmic to this position. On the other hand, when cysteines were engineered at positions 334, 335, and 337 in the outer vestibule, they were preferentially accessed in the closed state by externally applied $[Au(CN)_2]^-$, whereas they were nonreactive toward internally applied $[Au(CN)_2]^-$ in the absence of ATP, implicating a physical barrier between positions 344 and 337 along TM6 in the closed state. Taking our current understanding of the pore architecture and present data together, we conclude that, contrary to predictions based on the degraded ABC transporter hypothesis, the predicted narrowest section close to the middle of the pore could serve the role of a gate for CFTR.

Results

Because the presumed restricted region (residues 338–341 in TM6) depicted in Fig. 1*A* effectively prevents bulky MTS reagents from passing through the pore (15, 21, 22), to define the location of CFTR's gate, a channel-permeant probe that can traverse this part of the pore is needed. We chose pseudohalide anion $[Au(CN)_2]^-$ (dicyanoaurate) for the following reasons: First, although $[Au(CN)_2]^-$ is a linear molecule with a length of ~10 Å (29), the estimated cross-section diameter (3.4 Å) is slightly smaller than that of chloride (3.6 Å), enabling it to reside in the narrowest section of the pore (29, 30) and even cross the entire pore as a charge carrier (31). Second, using $[Au(CN)_2]^-$ as a thiol-reactive probe, Serrano et al. demonstrated that $[Au(CN)_2]^-$ can "irreversibly" modify an engineered cysteine in CFTR's anion permeation pathway (see ref. 32 for detailed chemistry between $[Au(CN)_2]^-$ and cysteine). To ensure the effectiveness and specificity of $[Au(CN)_2]^-$ in our system, we first tested its effect on wild-type (WT) cysless channels as a control. As shown in Fig. 1*B*, after macroscopic current of WT cysless channels in an inside-out patch was elicited with 2 mM ATP, the application of 1 mM $[Au(CN)_2]^-$ in the presence of ATP immediately decreased the current to a significant extent. The current readily resumed once $[Au(CN)_2]^-$ was removed, as predicted by the well-documented reversible blocking effect of $[Au(CN)_2]^-$ on CFTR (21, 29, 30). This result also reassures us that any residual effects after removal of $[Au(CN)_2]^-$ are due to the ligand exchange reaction between the introduced cysteines and the probe.

Exclusion of an Internal Gate for CFTR. Two previous reports (15, 16) demonstrated that cysteines engineered in the internal vestibule part of TM6 or TM12 can be modified by bulky MTS reagents in both the open state and the closed state. Here using $[Au(CN)_2]^-$, we obtained similar results. With a cysteine engineered at position 344, which is one helical turn below the intracellular end of the predicted narrow region (Fig. 1*A*), reaction rates in the absence and presence of ATP were measured by the following experimental protocols: In inside-out patches, after CFTR channels were fully activated by PKA and ATP, the patches were first exposed to two 3-s ATP pulses to ensure no obvious rundown or dephosphorylation before $[Au(CN)_2]^-$ was applied (Fig. 1*C*). Then the ATP was washed out for 8 s to allow channel closure. In the absence of ATP, the channels were subsequently exposed to 1 mM $[Au(CN)_2]^-$ for 3 s, followed by a 2-s washout of $[Au(CN)_2]^-$. Another 3-s ATP pulse was applied to activate the channels, and the mean current amplitude was measured. Twelve such cycles were performed in each recording so that we were able to quantify the reaction rate of 344C by $[Au(CN)_2]^-$ in the absence of ATP by measuring the mean current induced by ATP each time (Fig. 1*D*, red squares). In the same patch, a later exposure of the channels to 1 mM $[Au(CN)_2]^-$ in the presence of ATP decreased the current in two distinct phases. The fast one was interpreted as the blockade phase, similar to that observed with WT channels (Fig. 1*B*). On the other hand, the second phase, which took a much longer time to reach the steady state, was interpreted as the ligand exchange phase from which the reaction rate between 344C and $[Au(CN)_2]^-$ in the presence of ATP could be estimated (Fig. 1*D*, gray trace). The

calculated reaction rates of 344C by $[Au(CN)_2]^-$ in the absence and presence of ATP are 37 ± 4 /M/s (per molar per second) (n = 8) and 32 ± 5 /M/s (n = 14), respectively. Moreover, we carried out similar experiments on a mutant with a cysteine engineered at position 1148 in TM12 that has also been previously demonstrated to line the inner vestibule (Fig. S1) (16, 18). Interestingly, the reaction rate of 1148C without ATP (2,089 ± 130 /M/s, n = 6) was much faster than that with ATP (437 ± 66 /M/s, n = 9), suggesting a better access of 1148C in the closed state. Taken together, these results corroborate the conclusion that CFTR's gate does not reside in the internal vestibule (16).

State-Dependent Reactivity of T338C, F337C, and R334C Implicates the Location of a Gate for CFTR. The data presented above suggest that CFTR's gate(s) is located external to position 344. We next extended our experiments to cover positions external to I344 on TM6. Consistent with a previous report (21), internal $[Au(CN)_2]^-$ failed to react with the cysteine placed at position 341 (see Fig. S2 for details). We then moved on to introduce a cysteine at position 338, which lies at the external edge of the predicted narrow region (Fig. 1*A*). [Of note, this empirically defined external accessibility barrier is not subject to temperature changes (33).] As shown in Fig. 2*A*, the application of just 50 μM $[Au(CN)_2]^-$ in the presence of ATP abolished over 90% of the T338C–CFTR current in an inside-out patch, and this reduction of the current is attributed to the stable coordination between 338C and the probe because removal of $[Au(CN)_2]^-$ from the solution failed to recover the current. Fitting the current decay with a single exponential function yields a reaction rate of 752 ± 59 /M/s (n = 7). In addition, lowering cytoplasmic $[Cl^-]$ further speeds up this reaction rate (Fig. S3), hence suggesting that $[Au(CN)_2]^-$ and chloride may compete for the same pathway before reaching 338C. To the contrary, the macroscopic current of T338C–CFTR remained almost constant when $[Au(CN)_2]^-$ was perfused to the patch in the absence of ATP (Fig. 2*B*). Similar observations were made for F337C–CFTR and R334C–CFTR (Fig. S4 *A–D*). For reasons unclear at this juncture, application of 1 mM $[Au(CN)_2]^-$ to inside-out patches containing K335C–CFTR only resulted in reversible block, although this residue has been previously implicated as pore-lining (Fig. S4*E*) (21). In addition, 1 mM $[Au(CN)_2]^-$ applied in the absence of ATP also hardly altered the K335C–CFTR current in inside-out patches (Fig. S4*F*). Here we considered two possible explanations for our experimental results. First, a physical barrier (gate) for $[Au(CN)_2]^-$ exists between position 338 and the internal vestibule when the channel is closed. Second, side chains of residues 334, 335, 337, and 338 are not freely accessible to the probe in the closed state due to local steric interference, while the gate is located somewhere else.

Localization of a Gate for CFTR in Between I344 and F337. We reasoned that if the side chains of residues 334, 335, 337, and 338 indeed become inaccessible to the probe in the closed state due to some local conformational changes, lowering the open probability (P_o) will decrease the reaction rate when $[Au(CN)_2]^-$ is applied from the extracellular side of the channel. Our previous studies demonstrated that a disease-associated mutation G1349D could decrease the P_o of CFTR by ~10-fold (34) without affecting trafficking of the channel (34, 35); we thus engineered this mutation into R334C, K335C, F337C, and T338C backgrounds. As shown in Fig. S5, indeed, introducing the G1349D mutation into T338C–CFTR lowered the P_o and decreased the reaction rate by ~10-fold, which can be interpreted as a limited accessibility of the side chain of 338C in the closed state. However, the reaction rate of extracellularly applied $[Au(CN)_2]^-$ for the 337C/G1349D mutant is slightly but noticeably faster than that of the 337C mutant (Fig. S5*B*), suggesting that the 337C side chain is better exposed in the closed state.

This slight difference in reaction rates between single and double mutants was also seen for R334C, which is one helical turn external to positions 337. As shown in Fig. 3*A*, in the presence of forskolin, 20 μM external $[Au(CN)_2]^-$ readily abolished whole-cell R334C–CFTR currents. This effect was caused by reaction of 334C with the probe, as DTT, but not removal of $[Au(CN)_2]^-$, recovered the current. Similar experiments were performed with the double mutant R334C/G1349D (Fig. 3*B*). Fitting the current decays upon addition of $[Au(CN)_2]^-$ yielded the reaction rates of 403 ± 20 /M/s (n = 7) and 537 ± 56 /M/s (n = 6) for R334C and R334C/G1349D, respectively. Although the P_o of R334C–CFTR cannot be assessed due to a greatly reduced single-channel amplitude, by comparing macroscopic current amplitudes in a large number of patches (Fig. 3*E*), we verified a more than 10-fold decrease of P_o by introducing the G1349D mutation. Thus, these results suggest that the side chain of 334C is in fact more accessible to externally applied $[Au(CN)_2]^-$ in the closed state.

A more drastically preferential reactivity for a closed channel was observed with the cysteine placed at position 335. When 1 mM $[Au(CN)_2]^-$ was applied to the external side of the cell expressing K335C–CFTR mutants, the whole-cell current decreased in two steps (Fig. 3*C*). Fitting the current decay with a double exponential function yields the reaction time constant, from which the reaction rate was estimated as 56 ± 9 /M/s (n = 5). These results, together with the only blocking effect of 1 mM $[Au(CN)_2]^-$ being seen on K335C–CFTR in inside-out patches in the presence of ATP (Fig. S4*E*), indicate that the side chain of 335C is not well exposed in the open state. However, after G1349D was introduced into K335C–CFTR to lower its P_o, 50 μM $[Au(CN)_2]^-$ could readily react with 335C with a reaction rate of 1,809 ± 201 /M/s (n = 5) (Fig. 3*D*). Because the P_o of the double mutant is almost 11-fold lower than that of the single mutant (Fig. 3*E*), the simplest interpretation of these results is that 335C is much more accessible to external $[Au(CN)_2]^-$ in the closed state (also see data from inside-out patches on this double mutant; Fig. S6). This preferential reactivity of 334C, 335C, and 337C to external $[Au(CN)_2]^-$ in closed channels is in stark contrast to the fact that they are virtually inaccessible toward internally applied $[Au(CN)_2]^-$ in the absence of ATP. Therefore,

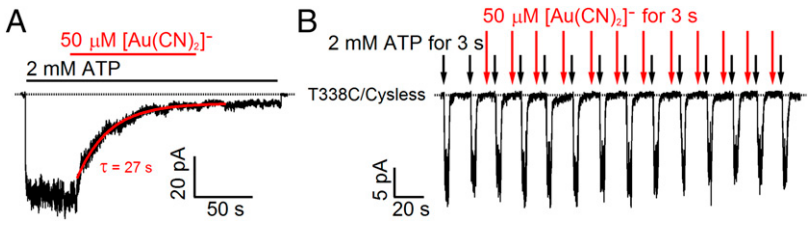

Fig. 2. State-dependent reactivity of T338C–CFTR to internal $[Au(CN)_2]^-$. (*A*) In the presence of ATP, internal $[Au(CN)_2]^-$ irreversibly decreases T338C–CFTR currents. The time constant τ was obtained by fitting the current decay with a single exponential function. (*B*) Contrary to that seen in *A*, T338C–CFTR currents were not significantly altered when the same concentration $[Au(CN)_2]^-$ was applied in the absence of ATP for a total of 36 s.

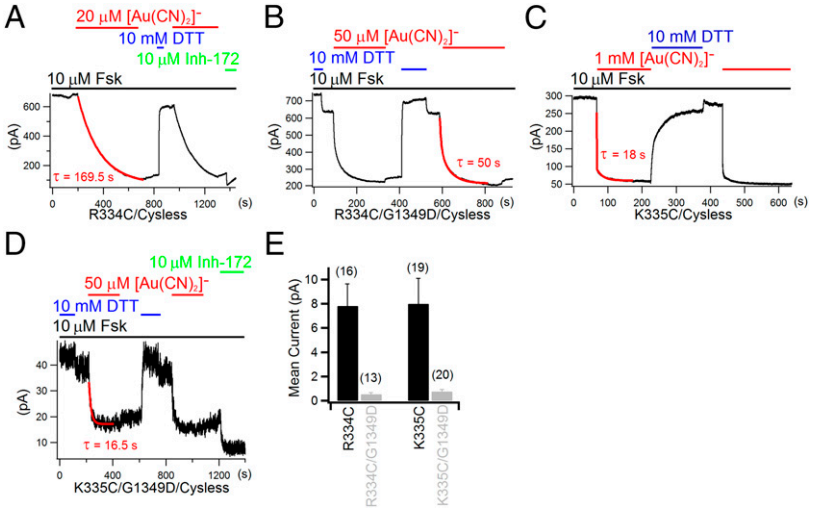

Fig. 3. Reaction of cysteines placed at positions 334 and 335 with external $[Au(CN)_2]^-$. (*A*) External application of 20 μM $[Au(CN)_2]^-$ diminished over 80% of forskolin (Fsk)-activated R334C–CFTR currents. After DTT reversed the effect brought by $[Au(CN)_2]^-$, the second application of the reagent abolished the current in a similar manner. The residual current after $[Au(CN)_2]^-$ is sensitive to a specific CFTR inhibitor (Inh-172). (*B*) $[Au(CN)_2]^-$ reacted with R334C/G1349D at a faster rate than that with R334C. Note a small current increase immediately after the removal of DTT. As reported by Liu et al. (36), this may be due to reactions of the thiol in a small fraction of the channels with trace metals, or nonspecific oxidation. (*C*) Reaction of K335C–CFTR channels with $[Au(CN)_2]^-$. For this construct, 1 mM $[Au(CN)_2]^-$ was applied because of a much slower reaction rate. The addition of 1 mM $[Au(CN)_2]^-$ led to a biphasic decay of forskolin-activated K335C–CFTR currents: a faster phase of blockade and a slower phase of ligand exchange reaction. (*D*) Reaction of K335C/G1349D–CFTR with $[Au(CN)_2]^-$. Fifty micromolar $[Au(CN)_2]^-$ was used, as the reaction rate for this double mutant is fast (see *Results* for details). Current decays in *A* and *D* were fitted with a single exponential function, whereas those in *B* and *C* were fitted with a double exponential function (red solid lines). Reaction time constants were indicated in each panel. (*E*) Comparisons of the mean current amplitude between R334C–CFTR and R334C/G1349D–CFTR and between K335C–CFTR and K335C/G1349D–CFTR in excised inside-out patches. Note that a ~10-fold difference in the mean current amplitude—hence a ~10-fold change in P_o—was seen with the introduction of the G1349D mutation, as shown previously for WT-CFTR (see *Results* for details). Number of patches is indicated above each bar.

considering the side chain of 344C is accessible by intracellular $[Au(CN)_2]^-$ regardless of whether the channel is open or closed (Fig. 1 *C* and *D*), we propose a gate residing in between positions 337 and 344 along TM6 for CFTR (Fig. 1*A*).

Discussion

Current Understanding of CFTR's Pore Architecture. Both functional and computational studies have led to a consensus that the CFTR pore is composed of three main compartments—namely, an internal vestibule, an external vestibule, and a narrow tunnel in between (Fig. 1*A*) (16, 20, 22, 26, 27, 29, 37). Although the field is awaiting the crystal structure of the whole CFTR protein, experiments using chemical probes of variable sizes have provided some insights into the dimensions of these three components. For the inner vestibule, it has been demonstrated that Texas red MTSEA with a head diameter of 13 Å can react with cysteines placed at positions as deep as near the narrow region in the closed state of CFTR (16). On the other hand, a strong voltage-dependent blockade of the open CFTR by sizable channel blockers such as glibenclamide (21.4 Å × 13.6 Å × 11.6 Å) further supports the notion that the inner vestibule of an open CFTR channel is large enough to accommodate those gigantic molecules (38). Although the inner vestibule has been extensively explored, much less is known for the outer vestibule. Besides MTS reagents (17, 21), few probes were reported to interact with the channel from the external side. Recently, GlyH-101, a high-affinity CFTR inhibitor (39), was reported to block the pore by lodging in the external vestibule close to positions 337 and 338 in TM6 (40). Interestingly, in the current study, we found that externally applied bulky Texas red MTSEA can modify the cysteine placed at position 338 (Fig. S7). Thus, the outer vestibule or at least the external pore entrance must also be spacious enough to accommodate the head group of this molecule. Quite contrary to these two vestibules, the bridging region has been proposed to be very narrow, as MTS reagents with a size of ~6 Å cannot pass through this section of the pore from either side of the membrane (15, 20, 21). Furthermore, by measuring the permeability ratio among different anions, Linsdell et al. proposed a size limit of ~5.3 Å for the CFTR pore (41). Collectively, a rough picture of the CFTR pore emerges: Two spacious electropositive vestibules attract anions to readily traverse a restricted tunnel that at a minimum serves as a size filter for CFTR's anion permeation pathway.

It is also interesting to note that both positively charged and negatively charged probes (e.g., MTSET and MTSES, respectively) have been shown to modify cysteines placed at position 341 from the intracellular side and position 338 from the extracellular side (Fig. 1*A*) (15, 21), suggesting that neither the internal nor external vestibule could serve as an effective charge discriminator for CFTR. This immediately raises the possibility that the predicted narrow tunnel spanning residues 338–341 may provide some sort of ion-selection mechanism. From the evolutionary point of view, CFTR may not need a stringent selectivity filter like the one seen in K^+ channels (42), as chloride ions are the predominant physiological anions. Indeed, it has been proposed that, by providing a nonspecified anion binding site against a background of dielectric polarizability, CFTR can effect a selectivity preference that is mostly determined by the size of permeant anions (29). Nonetheless, that both S341 and T338, whose side chains contain a hydroxyl group, dwell in this very region raises the possibility for these two residues to coordinate chloride in CFTR's pore—a strategy emulating the chemistry seen in the CLC proteins (43). Although mutations of T338 or S341 indeed significantly alter the permeation properties of CFTR (23, 44, 45), more studies seem warranted to tackle this important issue.

Identification of a Gate in the Middle of CFTR's Pore and Its Implications. Current cysteine scanning experiments on TM6 using a channel-permeant probe, $[Au(CN)_2]^-$, pinpoint a gate of CFTR to

a segment that coincides with the previously predicted narrow region of the pore for the following reasons. By measuring the reaction rates between engineered cysteines and $[Au(CN)_2]^-$ in different states as well as from different sides (data summarized in Table 1), we found the following: First, the cysteine placed at the position close to the intracellular end of the narrow region (e.g., position 344) can be accessed by cytoplasmic $[Au(CN)_2]^-$ irrespective of the gating state of the channel (Fig. 1*C*), supporting the conclusion that the internal vestibule does not harbor a gate. Second, 334C, 337C, and 338C engineered in the extracellular vestibule exhibit reactivity toward internal $[Au(CN)_2]^-$ only in the presence of ATP, implicating a physical barrier at the narrow region in the closed state of CFTR (Fig. 2 and Fig. S4). Third, three cysteines placed in the external vestibule (334C, 335C, and 337C) are all preferentially labeled in the closed state by external $[Au(CN)_2]^-$ (Fig. 3 and Fig. S5*B*), suggesting that the side chains of these three residues are still accessible when the channel closes. Collectively, these results can be explained by a minimal model depicting a gate located external to position 344 but internal to position 337.

Of note, by measuring the reaction rates of external $[Au(CN)_2]^-$ applied before and after cAMP-dependent activation of whole-cell CFTR channels, Norimatsu et al. reported a similar closed-state preference of accessibility for 334C (40). However, the state-dependent accessibility pattern of 337C in the current study strays from their results. It is worth noting that the strategies adopted in the current report—removing ATP in inside-out experiments and introducing a second mutation for whole-cell recordings—are meant to manipulate ATP-dependent gating of CFTR rather than to alter the phosphorylation status of the channel as used in Norimatsu et al. It will be interesting to investigate in the future if this technical difference may account for this discrepancy. Nevertheless, our observation that F337 is the innermost position wherein an introduced cysteine can be reached in the closed state by external $[Au(CN)_2]^-$ suggests that T338 should constitute the external end of the gate defined in the current study. On the other hand, if one accepts the idea that TM6 assumes an α-helical structure (15, 21), the cytoplasmic end of this gate can be further stipulated at position 341, as C344, located one helical turn internal to position 341, is equally accessible to intracellular $[Au(CN)_2]^-$ in the open and closed states. Then, the gate identified in the current study (T338–S341) coincides precisely with the predicted narrow region defined previously by SCAM studies with bulky MTS reagents (15, 21). That T338 is part of the gate can also explain why 338C shows open-state favored reactivity toward $[Au(CN)_2]^-$ applied from either side of the channel. Although the current results are consistent with an economic one-gate model for CFTR, with a limited structural understanding of this molecule, we cannot rule out the possibility of the presence of other gate(s). Especially in view of the evolutionary relationship between CFTR and ABC transporters, whether a gate exists in the external vestibule awaits further experimental explorations.

The picture that CFTR possesses a gate close to the middle of its ion-conducting pathway departs markedly from those well-appreciated structures of ABC proteins: two separate gates located at either end of a conduit where the substrate binds and traverses. Although the exact gating motion of CFTR's TMDs remains unclear, recent studies do provide evidence for a significant rearrangement of different TMs (20, 25) in addition to possible translational and rotational movements of individual TMs (15, 16, 46). Here, we propose that CFTR's pore-lining TMs may clog around the narrow region to craft a gate that ceases the chloride flow in the closed state. "Opening" of the channel involves rearrangements of TMs to grant a patency of this region for anion flow. This picture, albeit overtly simplified, not only explains why 338C shows strict open state-dependent modifications toward both internal and external $Au[(CN)]_2^-$, but also goes along with the results from computational simulations carried out by Norimatsu et al. In their study, although the same bottleneck region is wide enough to accommodate various anions, it can also pinch off to sever the continuous open pore (22). Evidently, more studies are needed to elucidate the molecular basis of CFTR gating. However, the notion that one single structural component may serve as both a gate and the selectivity filter distinguishes CFTR from other ABC proteins and therefore should be taken into account for future computational modelings of CFTR.

Materials and Methods

Mutagenesis and Channel Expression. All mutations were made in a cysless background construct and confirmed by DNA sequencing (DNA core, University of Missouri). Together with pEGFP-C3 (Takara Bio Inc.) that encodes the green fluorescent protein, the constructs were transfected into Chinese hamster ovary cells grown in DMEM with 10% (vol/vol) FBS for channel expression, using PolyFect reagent (QIAGEN) according to the manufacturer's instructions. Electrophysiological experiments were performed 2–7 d after transfection.

Electrophysiology.

Inside-out mode. Pipettes were pulled with a two-step vertical puller (Narishige) and polished using a homemade microforge to yield a resistance of 2–4 MΩ when placed in our bath solution. Before experiments, cells expressing different CFTR mutants were transferred into a chamber filled with bath solution containing (in mM) 145 NaCl, 5 KCl, 2 $MgCl_2$, 1 $CaCl_2$, 5 glucose, 5 Hepes, and 20 sucrose, with pH adjusted to 7.4 using NaOH. After a GΩ seal was made, the patch was excised into the inside-out configuration and the perfusion solution was changed to an inside-out perfusate containing (in mM) 150 N-Methyl-D-glucamine (NMDG)-Cl, 2 $MgCl_2$, and 10 Hepes, with pH adjusted to 7.4 using NMDG. In all inside-out experiments, pipettes were filled with a solution containing (in mM) 140 NMDG-Cl, 2 $MgCl_2$, 5 $CaCl_2$, and 10 Hepes, with pH adjusted to 7.4 using NMDG. To measure modification rates, a fast solution change system (SF-77B; Warner Instruments) was used to efficiently switch pipette tips among the outlets of a three-barrel glass, thus minimizing the delay in solution changes. All modification experiments were carried out after CFTR variants were fully activated with PKA and ATP.

Table 1. Summary of the reaction rates in response to intracellular and extracellular $[Au(CN)_2]^-$

Location	Residue	Intra. $[Au(CN)_2]^-$, ATP, /M/s	Intra. $[Au(CN)_2]^-$, no ATP, /M/s	Extra. $[Au(CN)_2]^-$, forskolin, /M/s	Extra. $[Au(CN)_2]^-$, forskolin, with G1349D, /M/s
Outside	*R334C*	*189 ± 39*	—	*403 ± 20*	*537 ± 56*
	K335C	—	—	*56 ± 9*	*1,809 ± 201*
	F337C	*437 ± 49*	—	*20 ± 3*	*32 ± 6*
	T338C	*752 ± 59*	—	*1,135 ± 166*	*118 ± 18*
Inside	I344C	32 ± 5	37 ± 4	—	—
	N1148C	437 ± 66	2,089 ± 130	—	—

Residues located extracellularly (extra.) to the predicted narrow region are in italics, and residues in roman type represent positions intracellularly (intra.) to this region. The reaction rates are presented as mean ± SEM (n = 4–14).

The membrane potential was held at –50 mV; downward deflections of the current trace represent channel opening. All of the data were recorded with a patch-clamp amplifier (EPC 10; HEKA), filtered with an 8-pole low-pass Bessel filter (100 Hz), and digitized at 500 Hz using Pulse software (V8.80; HEKA).

Whole-cell mode. Pipettes used for whole-cell recordings were pulled as described above. However, for an easier breaking-in to achieve the whole-cell mode, pipettes were not polished. The pipette resistance ranged between 1.5 MΩ and 3 MΩ when filled with a solution containing (in mM) 10 EGTA, 10 Hepes, 20 tetraethylammonium-Cl, 10 MgATP, 2 $MgCl_2$, 85 aspartate, 16 pyruvate, and 5.8 glucose, with pH adjusted to 7.4 using CsOH. The bath solution used was the same as the one used in inside-out experiments. After breaking in, cells were lifted from the bottom of the chamber and moved to the outlets of the three-barrel glass. The membrane potential was held at 0 mV; upward deflections of the current trace represent channel openings. Whole-cell CFTR currents were activated with forskolin before the application of $[Au(CN)_2]^-$. The signal was filtered at 100 Hz and digitized at 2 kHz. All experiments were performed at room temperature.

Reagents. Stock solutions of $[Au(CN)_2]^-$ (Sigma-Aldrich) were prepared as 10 mM. Before use, it was diluted into different concentrations (20 μM–1 mM) subject to different mutations. MTS reagents (Toronto Research Chemicals) were stored at –70° as 100-mM stock solutions. Each aliquot was diluted into 10 μM–2 mM for immediate use. All tubings for $[Au(CN)_2]^-$ and Texas red MTSEA were wrapped with tin foil due to the light sensitivity of the reagents. To ensure most cysteines were in the reduced form before each experiment, DTT (Sigma-Aldrich) was added into the PKA/ATP mixture for channel activation. CFTRinh-172 (inh-172) was kindly provided by Robert Bridges, Department of Physiology and Biophysics, Rosalind Franklin University, Chicago, with support from the Cystic Fibrosis Foundation Therapeutics. PKA and ATP were purchased from Sigma-Aldrich.

Data analysis. To obtain the modification time constant τ, in recordings where the CFTR current decays in one phase upon the application of $[Au(CN)_2]^-$, we fitted the current decay with a single exponential function using the Igor program (V4.07; WaveMetrics). A double exponential function was used to fit the current decay in recordings where a distinct two-phase current decay was seen. The secondary modification rate was calculated as $1/(\tau * \text{concentration of } [Au(CN)_2]^-)$. All data are presented as means ± SEM; *n* is the number of patches for each experiment.

ACKNOWLEDGMENTS. This work was supported by National Institutes of Health (NIH) Grant NIHR01DK55835 and Grant Hwang11P0 from the Cystic Fibrosis Foundation (to T.-C.H.). This investigation was conducted in a facility constructed with support from Research Facilities Improvement Program Grant C06 RR-01648901 from the National Center for Research Resources, NIH.

1. Ashcroft F, Gadsby D, Miller C (2009) Introduction. The blurred boundary between channels and transporters. *Philos Trans R Soc Lond B Biol Sci* 364(1514):145–147.
2. Jayaram H, Accardi A, Wu F, Williams C, Miller C (2008) Ion permeation through a Cl-selective channel designed from a CLC Cl-/H+ exchanger. *Proc Natl Acad Sci USA* 105(32):11194–11199.
3. Rees DC, Johnson E, Lewinson O (2009) ABC transporters: The power to change. *Nat Rev Mol Cell Biol* 10(3):218–227.
4. Jardetzky O (1966) Simple allosteric model for membrane pumps. *Nature* 211(5052): 969–970.
5. Dawson RJ, Locher KP (2006) Structure of a bacterial multidrug ABC transporter. *Nature* 443(7108):180–185.
6. Ward A, Reyes CL, Yu J, Roth CB, Chang G (2007) Flexibility in the ABC transporter MsbA: Alternating access with a twist. *Proc Natl Acad Sci USA* 104(48):19005–19010.
7. Aller SG, et al. (2009) Structure of P-glycoprotein reveals a molecular basis for poly-specific drug binding. *Science* 323(5922):1718–1722.
8. Hohl M, Briand C, Grütter MG, Seeger MA (2012) Crystal structure of a heterodimeric ABC transporter in its inward-facing conformation. *Nat Struct Mol Biol* 19(4):395–402.
9. Chen TY, Hwang TC (2008) CLC-0 and CFTR: Chloride channels evolved from transporters. *Physiol Rev* 88(2):351–387.
10. Dean M, Annilo T (2005) Evolution of the ATP-binding cassette (ABC) transporter superfamily in vertebrates. *Annu Rev Genomics Hum Genet* 6:123–142.
11. Riordan JR, et al. (1989) Identification of the cystic fibrosis gene: Cloning and characterization of complementary DNA. *Science* 245(4922):1066–1073.
12. Hwang TC, Sheppard DN (2009) Gating of the CFTR Cl- channel by ATP-driven nucleotide-binding domain dimerisation. *J Physiol* 587(Pt 10):2151–2161.
13. Jih KY, Hwang TC (2012) Nonequilibrium gating of CFTR on an equilibrium theme. *Physiology (Bethesda)* 27(6):351–361.
14. Gadsby DC, Nairn AC (1999) Control of CFTR channel gating by phosphorylation and nucleotide hydrolysis. *Physiol Rev* 79(1, Suppl):S77–S107.
15. Bai Y, Li M, Hwang TC (2010) Dual roles of the sixth transmembrane segment of the CFTR chloride channel in gating and permeation. *J Gen Physiol* 136(3):293–309.
16. Bai Y, Li M, Hwang TC (2011) Structural basis for the channel function of a degraded ABC transporter, CFTR (ABCC7). *J Gen Physiol* 138(5):495–507.
17. El Hiani Y, Linsdell P (2010) Changes in accessibility of cytoplasmic substances to the pore associated with activation of the cystic fibrosis transmembrane conductance regulator chloride channel. *J Biol Chem* 285(42):32126–32140.
18. Qian F, El Hiani Y, Linsdell P (2011) Functional arrangement of the 12th transmembrane region in the CFTR chloride channel pore based on functional investigation of a cysteine-less CFTR variant. *Pflugers Arch* 462(4):559–571.
19. Wang W, El Hiani Y, Linsdell P (2011) Alignment of transmembrane regions in the cystic fibrosis transmembrane conductance regulator chloride channel pore. *J Gen Physiol* 138(2):165–178.
20. Gao X, Bai Y, Hwang TC (2013) Cysteine scanning of CFTR's first transmembrane segment reveals its plausible roles in gating and permeation. *Biophys J* 104(4):786–797.
21. Alexander C, et al. (2009) Cystic fibrosis transmembrane conductance regulator: Using differential reactivity toward channel-permeant and channel-impermeant thiol-reactive probes to test a molecular model for the pore. *Biochemistry* 48(42):10078–10088.
22. Norimatsu Y, et al. (2012) Cystic fibrosis transmembrane conductance regulator: A molecular model defines the architecture of the anion conduction path and locates a "bottleneck" in the pore. *Biochemistry* 51(11):2199–2212.
23. McCarty NA, Zhang ZR (2001) Identification of a region of strong discrimination in the pore of CFTR. *Am J Physiol Lung Cell Mol Physiol* 281(4):L852–L867.
24. Wang W, El Hiani Y, Rubaiy HN, Linsdell P (2014) Relative contribution of different transmembrane segments to the CFTR chloride channel pore. *Pflugers Arch* 466(3):477–490.
25. El Hiani Y, Linsdell P (2014) Metal bridges illuminate transmembrane domain movements during gating of the cystic fibrosis transmembrane conductance regulator chloride channel. *J Biol Chem* 289(41):28149–28159.
26. Rahman KS, Cui G, Harvey SC, McCarty NA (2013) Modeling the conformational changes underlying channel opening in CFTR. *PLoS ONE* 8(9):e74574.
27. Mornon JP, Hoffmann B, Jonic S, Lehn P, Callebaut I (2014) Full-open and closed CFTR channels, with lateral tunnels from the cytoplasm and an alternative position of the F508 region, as revealed by molecular dynamics. *Cell Mol Life Sci*, in press.
28. Gadsby DC (2009) Ion channels versus ion pumps: The principal difference, in principle. *Nat Rev Mol Cell Biol* 10(5):344–352.
29. Smith SS, Steinle ED, Meyerhoff ME, Dawson DC (1999) Cystic fibrosis transmembrane conductance regulator. Physical basis for lyotropic anion selectivity patterns. *J Gen Physiol* 114(6):799–818.
30. Fatehi M, St Aubin CN, Linsdell P (2007) On the origin of asymmetric interactions between permeant anions and the cystic fibrosis transmembrane conductance regulator chloride channel pore. *Biophys J* 92(4):1241–1253.
31. Gong X, Burbridge SM, Cowley EA, Linsdell P (2002) Molecular determinants of Au(CN)(2)(-) binding and permeability within the cystic fibrosis transmembrane conductance regulator Cl(-) channel pore. *J Physiol* 540(Pt 1):39–47.
32. Serrano JR, et al. (2006) CFTR: Ligand exchange between a permeant anion ([Au(CN)2]-) and an engineered cysteine (T338C) blocks the pore. *Biophys J* 91(5):1737–1748.
33. Liu X, Dawson DC (2011) Cystic fibrosis transmembrane conductance regulator: Temperature-dependent cysteine reactivity suggests different stable conformers of the conduction pathway. *Biochemistry* 50(47):10311–10317.
34. Bompadre SG, Sohma Y, Li M, Hwang TC (2007) G551D and G1349D, two CF-associated mutations in the signature sequences of CFTR, exhibit distinct gating defects. *J Gen Physiol* 129(4):285–298.
35. Gregory RJ, et al. (1991) Maturation and function of cystic fibrosis transmembrane conductance regulator variants bearing mutations in putative nucleotide-binding domains 1 and 2. *Mol Cell Biol* 11(8):3886–3893.
36. Liu X, Alexander C, Serrano J, Borg E, Dawson DC (2006) Variable reactivity of an engineered cysteine at position 338 in cystic fibrosis transmembrane conductance regulator reflects different chemical states of the thiol. *J Biol Chem* 281(12):8275–8285.
37. Linsdell P (2014) Functional architecture of the CFTR chloride channel. *Mol Membr Biol* 31(1):1–16.
38. Sheppard DN, Robinson KA (1997) Mechanism of glibenclamide inhibition of cystic fibrosis transmembrane conductance regulator Cl- channels expressed in a murine cell line. *J Physiol* 503(Pt 2):333–346.
39. Muanprasat C, et al. (2004) Discovery of glycine hydrazide pore-occluding CFTR inhibitors: Mechanism, structure-activity analysis, and in vivo efficacy. *J Gen Physiol* 124(2):125–137.
40. Norimatsu Y, et al. (2012) Locating a plausible binding site for an open-channel blocker, GlyH-101, in the pore of the cystic fibrosis transmembrane conductance regulator. *Mol Pharmacol* 82(6):1042–1055.
41. Linsdell P, et al. (1997) Permeability of wild-type and mutant cystic fibrosis transmembrane conductance regulator chloride channels to polyatomic anions. *J Gen Physiol* 110(4):355–364.
42. Morais-Cabral JH, Zhou Y, MacKinnon R (2001) Energetic optimization of ion conduction rate by the K+ selectivity filter. *Nature* 414(6859):37–42.
43. Dutzler R, Campbell EB, Cadene M, Chait BT, MacKinnon R (2002) X-ray structure of a ClC chloride channel at 3.0 A reveals the molecular basis of anion selectivity. *Nature* 415(6869):287–294.
44. Linsdell P, Zheng SX, Hanrahan JW (1998) Non-pore lining amino acid side chains influence anion selectivity of the human CFTR Cl- channel expressed in mammalian cell lines. *J Physiol* 512(Pt 1):1–16.
45. Linsdell P (2001) Relationship between anion binding and anion permeability revealed by mutagenesis within the cystic fibrosis transmembrane conductance regulator chloride channel pore. *J Physiol* 531(Pt 1):51–66.
46. Wang W, Linsdell P (2012) Relative movements of transmembrane regions at the outer mouth of the cystic fibrosis transmembrane conductance regulator channel pore during channel gating. *J Biol Chem* 287(38):32136–32146.